Electronic phase separation near the superconductor-insulator transition of $Nd_{1+x}Ba_{2-x}Cu_3O_{7-\delta}$ thin films studied by an electric-field-induced doping effect

M. Salluzzo,[1,*] A. Gambardella,[1] G. M. De Luca,[1] R. Di Capua,[1,2] Z. Ristic,[1,3] and R. Vaglio[1,3]
[1]*CNR-INFM COHERENTIA, Complesso di Monte S. Angelo, Via Cinthia, 80126 Napoli, Italy*
[2]*Dipartimento S.pe.S., Università del Molise, Via De Sanctis, 86100 Campobasso, Italy*
[3]*Dipartimento di Scienze Fisiche, Università di Napoli "Federico II," Complesso di Monte S. Angelo, Via Cinthia, 80126 Napoli, Italy*
(Received 6 August 2008; published 27 August 2008)

We report a detailed study of the transport properties of $Nd_{1+x}Ba_{2-x}Cu_3O_{7-\delta}$ thin films with doping changed by field effect. The data cover the whole superconducting to insulating transition and show remarkable similarities with the effect of chemical doping in high critical temperature superconductors. The results suggest that the add-on of carriers is accompanied by an electronic phase separation, independent on the details of the doping mechanism.

DOI: 10.1103/PhysRevB.78.054524 PACS number(s): 74.78.Bz, 74.25.Dw

I. INTRODUCTION

Electronic phase separation is a very general phenomenon in which a structurally and chemically homogeneous system shows instability toward the realization of a uniform electronic state. In manganites magnetic-metallic and paramagnetic-insulating phases may coexist near well defined compositions and temperature ranges.[1] In the high critical temperature superconductors (HTS) signatures of phase separation have been reported, in particular around the superconducting-insulating transition (SIT). However it is presently unclear whether these phenomena are a consequence of a purely electronic instability or they are originated by the disorder associated with the doping mechanism typical of cuprates. Indeed it is well established that the so-called parent compounds, being stoichiometric with an antiferromagnetic ground state, become superconductors through an introduction of nonstoichiometric addition of "impurity" ions, i.e., oxygen or cations that are randomly distributed within the lattice in the layers adjacent to the CuO_2 planes. Evidences of superconducting and nonsuperconducting regions coexisting at the nanoscale level at low temperatures come from scanning tunneling spectroscopy (STS),[2] neutron-diffraction,[3] and resonant x-ray inelastic scattering[4] experiments. STS studies have shown an apparent correlation between the location of dopant oxygen ions and the suppression of the superconducting state in $Bi_2Sr_2CaCu_2O_8$.[5] More recently, direct STS imaging reported the realization of short-range ordered "electronic cluster glasses" (ECG), i.e., an ordered distribution of carriers, around the critical doping of 0.05 holes/CuO_2 plane in two quite different underdoped cuprates, namely, $Ca_{1.88}Na_{0.12}CuO_2Cl_2$ and $Bi_2Sr_2Dy_{0.2}Ca_{0.8}Cu_2O_8$.[6]

In this paper we address the issue of the phase separation around the SIT of $Nd_{1+x}Ba_{2-x}Cu_3O_7$ (NdBCO) cuprate by using the electric-field effect doping. The electric-field effect is a very interesting way to change electronic properties of a material without modifying the structure and the chemical disorder, a concept successfully demonstrated in amorphous superconductors,[7] as well as HTS thin films.[8–10] Recently, we showed that the microscopic mechanism leading to the doping of NdBCO is very similar to the chemical doping; the charges induced are mainly created in the CuO chains (in the charge reservoir) and then partially transferred to the CuO_2 planes.[11] This is analogous to the general mechanism governing the charge transfer in the whole HTS family. However, by using the electric-field effect, the chemical disorder is frozen, and we may act on the SIT by changing the carrier density alone. We will show that the induced carriers arrange in the system producing changes in the temperature dependence of the resistivity very similar to the effect of chemical doping. Moreover, we will show that the doped holes are distributed in a way consistent with an intrinsic electronic phase-separation scenario.

II. FIELD EFFECT DEVICES FABRICATION AND CHARACTERIZATION

The NdBCO films were deposited by high oxygen pressure diode sputtering on 10×10 mm^2 $SrTiO_3$ (100) (STO) 0.5-mm-thick single crystals. The substrates were etched in a buffered HF solution (pH=5.5) and annealed, just before the deposition, at 950 °C in pure oxygen (99.99%) flow for 1 h in order to clean and reconstruct the terrace structure. The substrates have been characterized by several techniques. Shear force and AFM topography measurements, performed in contact mode, show well ordered single terminated surfaces. Such surface structure was checked by grazing incidence x-ray diffraction (GXID), which shows that the surface is almost completely TiO_2 terminated.[12]

NdBCO thin films have been grown on the top of these TiO_2 surfaces. The ultrahigh vacuum (UHV) sputtering system base pressure was always below 5×10^{-7} Pa before the deposition. Pure O_2 (99.99%), with a small percentage of Ar, composes the sputtering gas. Optimized NdBCO films were deposited at a total pressure of 2×10^2 Pa, made by 95% of oxygen and 5% of argon. The optimum deposition temperature was 930 °C. After the deposition the sample is oxygenated at 500 °C in 6×10^4 Pa of O_2 for 1 h.

The structure of NdBCO films is pseudotetragonal (and not twinned) and the in-plane lattice is perfectly matched with STO.[13] The samples retain a long-range ordered structure also in the thinnest films. Rocking curves around the (001) and (005) reflections of all the film deposited are char-

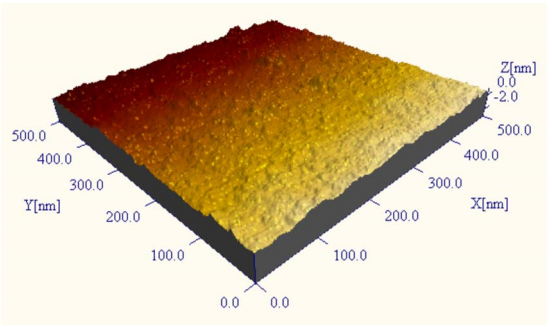

FIG. 1. (Color online) Noncontact atomic force microscopy of a 3-nm-thin NdBCO films deposited on TiO_2 terminated STO. The range of the vertical scale corresponds to the film thickness. The surface is extremely flat with an rms roughness of 0.1 nm.

acterized by a full width at half maximum of 0.030° and 0.080°, respectively, comparable to the resolution of our laboratory diffractometer. This result indicates small orientation misalignment between individual islands in each sample. X-ray reflectivity measurements show that even 2 unit cell (u.c.) thick-films show diffraction features typical of high structural quality samples. The film thickness is then determined experimentally with high accuracy from the period of the oscillation fringes.

In-plane long-range structure is checked by GXID through (H,K) maps around the (0,0,0.05) reflection, which exhibit finite fringing oscillation due to the characteristic terrace widths induced by the stepped well ordered substrate. The period corresponds exactly to the terrace width measured by AFM. Consequently, the crystalline quality of our NdBCO films is comparable to that of the STO single crystals.

The field effect structures deposited *in situ* in order to optimize each interface, consisted of a thin NdBCO (001) film of current and voltage evaporated gold pads realized by a shadow mask technique (the distance between the current and voltage pads are, respectively, 200 and 20 μm), and a gate electrode on the back of the 0.5-mm-thick STO substrate.

To avoid oxygen losses, an amorphous insulating NdBCO layer is grown at room temperature on the top of the structure. The unprotected surface of NdBCO films exhibits a structural relaxation after several days of exposition to the atmosphere (consistent with oxygen loss from the chains). Consequently the capping layer represents a protection necessary for the many measurements that should be done. With the NdBCO amorphous layer the sample is stable for months.

We performed noncontact atomic force microscopy (NC-AFM) characterization of our devices using an Omicron variable temperature AFM (VT-AFM) operating in ultrahigh vacuum. Figure 1 shows the morphology of a 2.5 u.c. NdBCO film before the deposition of the amorphous overlayer. The sample is extremely flat and is composed by two-dimensional (2D) well connected islands characterized by step-edge heights of the order of 0.4 nm, i.e., 1/3 of one unit cell. Previous detailed investigation have demonstrated that such growth mode is typical of Nd-rich NdBCO thin films

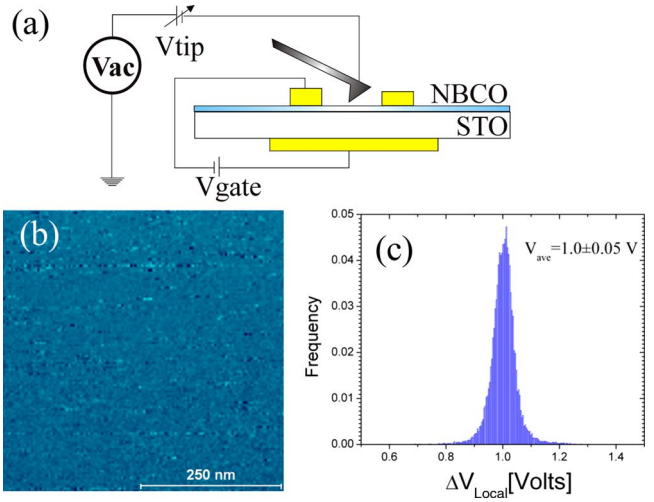

FIG. 2. (Color online) (a) Experimental setup used for the electrostatic force microscopy measurements. (b) Map of the local potential difference between the sample and the tip on a 500 $\times$500 nm^2 area; (c) histogram representation of the local potential map showing an average value of 1.0 V with a dispersion of 60 mV on the whole area.

and actually it is one of the reason of the reduced number of morphological defects observed in these samples compared to $Y_1Ba_2Cu_3O_7$ films.[14] The root-mean-square (rms) roughness on 2×2 μm^2 area is of the order of 0.1 nm.

To address the question of a possible spatial inhomogeneous charge distribution induced by a not uniform applied electric field, we performed electrostatic force microscopy (EFM) measurements on a 1 u.c. NdBCO thin film deposited on STO substrate, in order to investigate the electric-field distribution in the sample under the application of a gate voltage. EFM has been performed by the Omicron VT-AFM in UHV. The experimental configuration is schematically shown in Fig. 2(a). The gate electrode is deposited on the back side of the NdBCO/STO strip, while drain-source contacts are deposited on the top of the NdBCO film, which is grounded on one side. The same geometry is used during the transport measurements. An applied gate voltage of 100 V generates an electric field inside the 1 u.c. NdBCO. EFM measurements have been performed by applying a voltage modulation at a frequency ω=2.5 kHz (the resonant frequency of our cantilever is about 315 kHz). The normal force is then modulated by the electric field, giving a component F_ω at the modulation frequency. The real part of this signal is then measured by a lock-in. It turns out that F_ω is a linear function of the dc voltage on the tip, V_{tip}, and obeys the simplified expression;

$$F_\omega = \frac{\partial C}{\partial z}(V_{\text{tip}} - \Phi_{\text{local}} - \Phi_{\text{tip}})V_{\text{ac}},$$

where $\Phi_{\text{local}}-\Phi_{\text{tip}}$ is the contact potential difference between the sample and the tip, V_{ac} is the modulation amplitude, and C is local capacitance of the tip-sample system. Spectroscopic maps of F_ω at different values of V_{tip} have been acquired by measuring locally F_ω vs V_{tip} (open loop). From

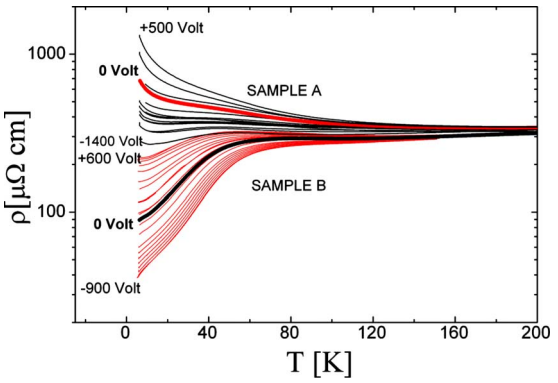

FIG. 3. (Color online) Temperature and field effect dependence of the resistivity in sample A (2.5 u.c.) and sample B (3.0 u.c.) NdBCO field effect devices. Thick gray (red online) and black lines are the zero-field data for sample A and sample B, respectively. The gate voltage dependence is plotted as thin black lines for sample A and thin gray (red online) for sample B.

these data, we have obtained the local potential difference between the sample and the tip, determined by the values of V_{tip} that nullify F_ω. An example of a spectroscopic map of $\Phi_{\text{local}}-\Phi_{\text{tip}}$ is shown in Fig. 2(b) together with a corresponding histogram [Fig. 2(c)]. The local potential difference is around 1 V and its spread is lower than 100 mV. Similar variation of the local potential are measured in the same area without the gate voltage applied, proving that the local potential on the sample is constant. An inhomogeneous distribution of the charges at the interface, for example at the step edge or at the grain boundary, would produce a modification of the local potential on the sample that should be observed by the EFM measurement. From these results we conclude that the electric field is homogeneous even at small scale (10–20 nm).

III. TRANSPORT MEASUREMENTS ON THE FIELD EFFECT DEVICES

Samples made of 2.5 and 3.0 u.c. are routinely grown and reproducibly show different transport properties. In particular a superconducting to insulating transition due the thickness effect is observed on these samples. For all temperatures and gate voltages reported here, the transport data were acquired at the strict linear-response regime.

In Fig. 3 the temperature and electric-field dependence of the resistivity of 2.5 u.c. sample A and of 3 u.c. sample B are shown. The results obtained are typical of devices deposited in similar deposition conditions. Sample A shows an insulating temperature dependence at zero electric field with a slight change in the slope of the characteristic semiconducting behavior around 40 K and an increase in the curvature at lower temperatures. On the contrary, sample B shows a metallic temperature dependence of the resistance, a minimum at about 100 K, a peak at about 75 K, and a superconducting transition that is incomplete. These characteristics indicate the presence of different competing conducting channels. A complete superconducting transition is observed only in 3.5 u.c. (at about 10 K) and in 4 u.c. samples (around 25 K).

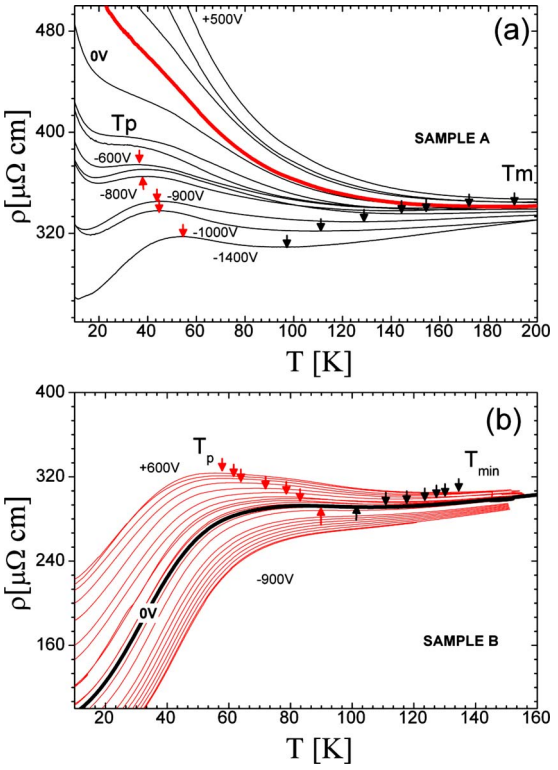

FIG. 4. (Color online) Temperature and field effect dependence of the resistivity in (a) sample A and (b) sample B shown on a scale that emphasizes the main features, i.e., the presence of a field dependent minimum T_{min} (black arrow) and of a maximum T_p (gray arrow; red arrow online). Thick gray (red online) and black lines are the zero-field data for sample A and sample B, respectively. Note the metal-insulator transition at high temperature observed in sample A.

The application of a gate voltage (V_g) produces continuous changes in the temperature dependence of the resistivity. In sample A we observe an evolution from a fully insulating characteristic at positive V_g to an incomplete transition to the superconducting state at lower temperatures for the highest negative value achieved of $V_g=-1400$ V. Notably at higher temperatures there is a gradual change from an insulating to a metallic temperature dependence of the resistivity that gives rise to a minimum and a peak before the occurrence of the superconducting transition [see Fig. 4(a)]. Analogously, the thicker sample B at positive gate voltages shows the presence of competing phases—with a metallic temperature dependence prevailing at high temperatures—a minimum, and a peak before the metallic fraction become superconducting [see Fig. 4(b)]. The temperatures at which the minimum (T_{min}) and the maximum (T_p) occur change with the electric field.

From the experimental data we have built a temperature vs field effect doping phase diagram, obtained by plotting the first derivative of the resistivity of the samples as a function of the gate voltage (Fig. 5). Different regions of the phase diagram are defined by the experimental T_p and T_{min} temperatures for each gate voltage. From Fig. 5 we can notice that T_{min} shifts to higher (lower) values by decreasing (increasing) the number of holes, i.e., by application of positive

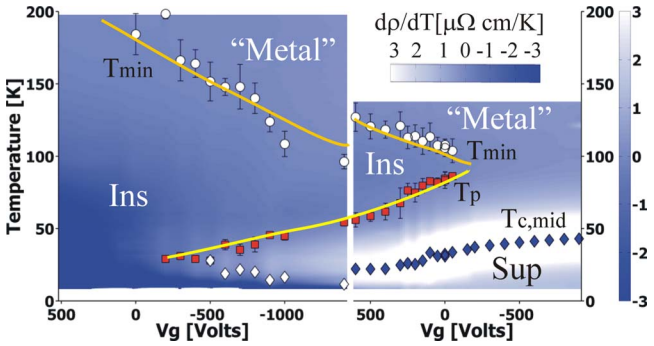

FIG. 5. (Color online) Field effect doping phase diagram around the superconducting-insulating transition of NdBCO films deduced from the data. The color map is the first-order derivative of the resistivity. Different regions of the phase diagram are separated by the experimental $T_{\min}$ (white circles) and T_p (gray squares; red squares online). Sup stands for superconducting and Ins stands for insulating. Blue diamonds are the T_c corresponding to the midpoint transition values, while additional white diamonds are the points where a reentrant SIT occurs. Finally the yellow dashed lines are guides for eyes.

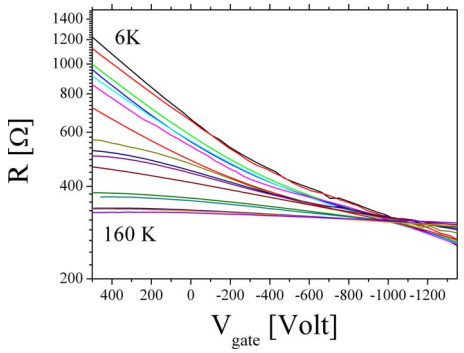

FIG. 6. (Color online)R vs V_{gate} isotherms for sample A across the SIT. A well defined crossing point is observed for the critical values of R_c=318 Ω and V_{gate}=−1000 V.

(negative) gate voltages. On the contrary, the position of the peak, T_p, increases with injection of holes. Both features, T_p and $T_{\min}$, merge at the doping corresponding to a fully metallic behavior. T_p is not the critical temperature of the superconducting regions in the sample, but its "field effect doping" dependence is qualitatively similar to well-known dependence of T_c by chemical doping. Moreover, we note that the point of maximum slope around the transition, normally assigned to the midpoint critical temperature $T_{c,\text{mid}}$, is proportional to T_p and has the same gate voltage dependence, in agreement with the analysis presented in Ref. 15. There T_p and T_c were effectively found to be proportional in the case of $Bi_2Sr_{2-x}La_xCaCu_2O_8$ thin films.

The similarity between the field effect and chemical doping phase diagrams near the SIT transition is remarkable. The characteristic temperature and chemical doping dependence of the resistivity has been observed in other HTS superconductors, i.e., in $Bi_2Sr_{2-x}La_xCaCu_2O_8$, $YBa_2Cu_3O_7$ and $La_{1-x}Sr_xCu_2O_4$ crystals and films.[15–18] This is a further proof that field effect and chemical dopings have a common microscopic mechanism.

IV. DISCUSSION AND CONCLUSIONS

We now turn to the discussion of the origin of the superconducting-insulating transition. The SIT in two-dimensional superconductors tuned by magnetic field, disorder, or doping are believed to be examples of continuous quantum phase transitions. The HTS are quasi-two-dimensional superconductors and consequently a SIT on these materials could belong to this category. The most striking evidence of a quantum phase transition in 2D films is the finite-size scaling of the experimental observable as a function of a critical parameter. In particular, the scaling theory states that the resistance R of 2D samples, above and below a critical value K_c of a tuning parameter K, should obey the functional form,

$$\frac{R}{R_c} = F\left[\frac{|K-K_c|}{T^{\nu z}}\right].$$

Here F is an unknown function and R_c is the value of the resistance at the critical point. Concerning the functional form of F, ν is the correlation length critical exponent and z is the dynamical critical exponent. While in amorphous BCS superconductors successful finite-size scaling analysis were reported,[19] this is not the case for the HTS.

We have tried to apply the finite-size scaling analysis to our data. In our case, the tuning parameter is the gate voltage. To determine the critical point, we have plotted the drain to source resistance vs gate voltage isotherms for sample A, where a change from an insulating to a superconducting transition is effectively observed. As shown in Fig. 6, there is a well defined crossing point occurring at about V_c=−1000 V and R_c=318 Ω. As a second step, we have assumed that sample B at V_g=+600 V and sample A at V_g=−1400 V have a similar doping. This hypothesis is reasonable since T_p and the high-temperature resistances of the two samples are similar.

Our analysis revealed that the curves failed to scale in a wide temperature range for different choices of the scaling parameters (Fig. 7). This happens especially for the positive gate voltages in sample B and the negative gate voltages in sample A, i.e., in the transition region. Similar results are obtained by using the induced charge (measured simultaneously to the resistance), instead of the gate voltage, as tuning parameter. It is therefore evident that finite scaling in the electric-field-induced SIT transition in underdoped NdBCO films is not satisfying. It is likely that, since in the HTS the onset of the phase transition occurs at relatively high temperatures, quantum effects, which of course have an important role in the physical phenomena, could be masked by thermodynamic fluctuations.

For this reason, we have built a phenomenological two-component model of the conductivity that has the ability to explain the main features in the data. One component, G_S, corresponds to a superconducting phase having a given T_c and the other G_I corresponds to an insulating phase. We have assumed that the insulating and superconducting components are in series and in parallel. The resistance R then can be written using the following expression:

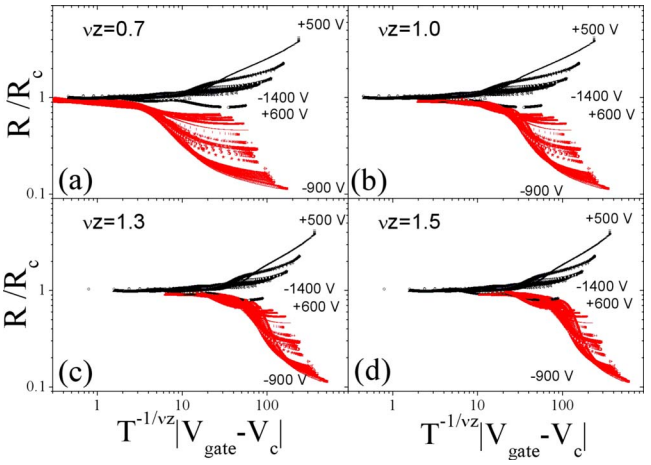

FIG. 7. (Color online) Scaling of the experimental resistivity curves plotted as R/R_c vs $\frac{|V_g-V_c|}{T^{\nu z}}$ for different values of the critical exponent: (a) $\nu z=0.7$, (b) $\nu z=1.0$, (c) $\nu z=1.3$, and (d) $\nu z=1.5$.

$$R = \frac{1}{(1-x)\cdot G_I + x\cdot G_{SI}}, \tag{1}$$

with

$$\frac{1}{G_{SI}} = \frac{(1-y)}{G_I} + \frac{y}{G_S}. \tag{2}$$

In Eqs. (1) and (2) x and y are related to the fraction of superconducting and insulating channels contributing to the transport. We do not explicitly refer to a precise microscopic model for the two phases since it is not possible to discriminate from the data any evidence in favor of one particular model. The data on sample A, obtained with $V_g=+500$ V, are compatible with quantum weak localization, i.e., a $\log(T/T_0)$ term, but a power-law expression of the form $G_I = a\cdot T^q$ gives a better fit ($q=0.42$). This weak insulating characteristic evolves into a 2D Mott insulating behavior in thinner samples, in agreement with the analysis reported in Ref. 15. Concerning the superconducting phase, we use an Aslamazov-Larkin term $G_s=\frac{b}{T/T_c-1}$ due to the superconducting thermal fluctuations. The inclusion of quantum effects, like Maki–Thompson, and a more rigorous treatment of the superconducting fluctuation around the transition are beyond the scope of the work.

In the fitting procedure we have used two methods. As first attempt we have fixed the parameter x and y to be able to qualitatively reproduce the results on sample A with $V_{\text{gate}}=-1000$ V, and then we have fitted all the data by living all the other parameters free to change. We found it impossible to obtain a reasonable description of the experimental results by using this method. We underline that independently on the specific functional form used to represent the conductivity of the superconducting and the insulating regions, we have found extremely hard to explain the experimental results by changing only the parameters that define the characteristics of the two phases, without modifying their ratio. As a second strategy, we have fixed parameters a and exponent q (from the fit on sample A at

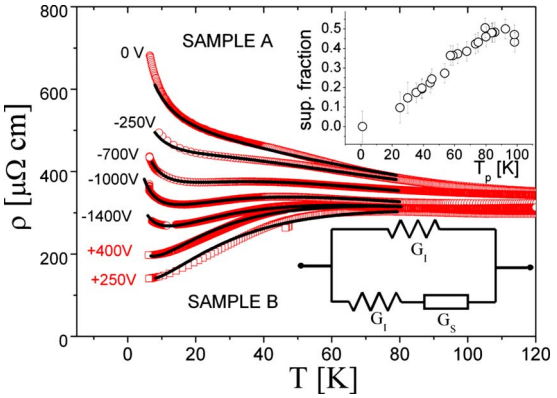

FIG. 8. (Color online) Comparison between the experimental resistivity [sample A open red (gray online) circles and sample B red (gray online) squares] and the model (black continuous lines) for selected gate voltages as indicated in the figure (see text). In the inset the superconducting fraction deduced from the fitting parameters in function of the experimental peak temperature T_p.

$V_g=+500$ V, the most insulating curve), keeping the ratio between T_c and the experimental T_p equal to $T_c/T_p \simeq 0.1$. As shown in Fig. 8, a good agreement between the data and the model is obtained in this case. The result supports the idea that to explain the SIT it is necessary to assume that the superconducting fraction f_s, given by x times y in the model, is a function of the field effect doping. In particular, f_s consistently increases with T_p (see inset of Fig. 8). In sample B, at negative gate voltages higher than -100 V, the peak disappears in the experimental curve. As consequence T_c in the model should become a free parameter. We consistently verified that in the model the superconducting fraction tends toward one in sample B at the highest gate voltages.

There are two main possible scenarios emerging from the data. We start from the observation that at $V_g=0$ the samples are in an inhomogeneous electronic state. In the first scenario, the phase separation is attributed to the chemical disorder only, which remains fixed while the electric field is changed. The induced charges would simply switch insulating regions into superconducting ones, and vice versa. In the other scenario, while the charges induced by the field are mainly distributed in the charge reservoir[11] uniformly (Fig. 2), the carriers transferred to the CuO_2 plane are not, i.e., the carrier doping of the CuO_2 plane is, around the SIT, intrinsically inhomogeneous. In favor of the latter scenario, there are the following experimental facts: the signatures of the inhomogeneous state in sample A fully disappear by applying sufficiently high positive gate voltages, i.e., taking out holes from the sample. This means that for a sufficiently low carrier density, the sample becomes electronically homogeneous even with the chemical disorder remaining unaffected. Simultaneously in sample B, by adding a sufficient number of carriers, the peak and the minimum in the temperature dependence of the resistance, being the signatures of competing phases, disappear as well. Consequently the chemical disorder alone cannot explain the changes in the inhomogeneous state obtained by electric-field effect, as well as does not explain why, by the electric field, it is possible to transform an otherwise inhomogeneous system into a homoge-

neous one, both on the insulating and on the superconducting side of the phase diagram. We underline, on the other hand, that the phenomenology of the electric-field effect is identical to that of the chemical doping. The results are consequently consistent with a model in which the charges induced by field effect naturally distribute in hole-rich and hole-poor regions, a scenario proposed also to explain the effect of chemical doping.[20]

In conclusion, in this paper we have reported a detailed study of the field effect induced superconducting-insulating transition in $Nd_{1+x}Ba_{2-x}Cu_3O_{7-\delta}$ thin films. We demonstrated that the details of the temperature dependence of the resistivity around the SIT are similar in the case of field effect and chemical dopings. The analysis of the data supports the idea that holes doped in the system near the SIT lead to an electronic phase-separation state composed by insulating and superconducting region, coexisting at the same time.

ACKNOWLEDGMENT

M.S., A.G., G.M.D.L., and R.V. acknowledge the support from the EU under the project Nanoxide, Contract No. 033191.

*salluzzo@na.infn.it

[1] E. Dagotto, *Nanoscale Phase Separation and Colossal Magnetoresistance* (Springer, Berlin, 2003).
[2] S. H. Pan, J. P. O'Neal, R. L. Badzey, C. Chamon, H. Ding, J. R. Engelbrecht, Z. Wang, H. Eisaki, S. Uchida, and A. K. Guptak, Nature (London) **413**, 282 (2001).
[3] J. M. Tranquada, B. J. Sternlieb, J. D. Axe, Y. Nakamura, and S. Uchida, Nature (London) **375**, 561 (1995).
[4] P. Abbamonte, A. Rusydi, S. Smadici, G. D. Gu, G. A. Sawatzky, and D. L. Feng, Nat. Phys. **1**, 155 (2005).
[5] K. McElroy, Jinho Lee, J. A. Slezak, D.-H. Lee, H. Eisaki, S. Uchida, and J. C. Davis, Science **309**, 1048 (2005).
[6] Y. Kohsaka, C. Taylor, K. Fujita, A. Schmidt, C. Lupien, T. Hanaguri, M. Azuma, M. Takano, H. Eisaki, H. Takagi, S. Uchida, and J. C. Davis, Science **315**, 1380 (2007).
[7] C. H. Ahn, A. Bhattacharya, M. Di Ventra, J. N. Eckstein, C. Daniel Frisbie, M. E. Gershenson, A. M. Goldman, I. H. Inoue, J. Mannhart, Andrew J. Millis, Alberto F. Morpurgo, Douglas Natelson, and Jean-Marc Triscone, Rev. Mod. Phys. **78**, 1185 (2006).
[8] G. Yu. Logvenova, C. W. Schneider, J. Mannhart, and Yu. S. Barash, Appl. Phys. Lett. **86**, 202505 (2005).
[9] A. Rufenacht, J.-P. Locquet, J. Fompeyrine, D. Caimi, and P. Martinoli, Phys. Rev. Lett. **96**, 227002 (2006).
[10] D. Matthey, N. Reyren, J.-M. Triscone, and T. Schneider, Phys. Rev. Lett. **98**, 057002 (2007).
[11] M. Salluzzo, G. Ghiringhelli, J. C. Cezar, N. B. Brookes, G. M. De Luca, F. Fracassi, and R. Vaglio, Phys. Rev. Lett. **100**, 056810 (2008).
[12] A. Fragneto, G. M. De Luca, R. Di Capua, U. Scotti di Uccio, M. Salluzzo, X. Torrelles, Tien-Lin Lee, and J. Zegenhagen, Appl. Phys. Lett. **91**, 101910 (2007).
[13] M. Salluzzo, G. M. de Luca, D. Marré, M. Putti, M. Tropeano, U. Scotti di Uccio, and R. Vaglio, Phys. Rev. B **72**, 134521 (2005).
[14] M. Salluzzo, C. Aruta, I. Maggio-Aprile, Ø. Fischer, J. Zegenhagen, and S. Bals, Phys. Status Solidi A **186**, 339 (2001).
[15] Seongshik Oh, Trevis A. Crane, D. J. Van Harlingen, and J. N. Eckstein, Phys. Rev. Lett. **96**, 107003 (2006).
[16] Kouichi Semba and Azusa Matsuda, Phys. Rev. Lett. **86**, 496 (2001).
[17] Y. Ando, G. S. Boebinger, A. Passner, T. Kimura, and K. Kishio, Phys. Rev. Lett. **75**, 4662 (1995).
[18] S. Ono, Y. Ando, T. Murayama, F. F. Balakirev, J. B. Betts, and G. S. Boebinger, Phys. Rev. Lett. **85**, 638 (2000).
[19] K. A. Parendo, K. H. Sarwa B. Tan, and A. M. Goldman, Phys. Rev. B **73**, 174527 (2006), and references therein.
[20] V. J. Emery, S. A. Kivelson, and H. Q. Lin, Phys. Rev. Lett. **64**, 475 (1990).